ARCHIVES OF ELECTRICAL ENGINEERING VOL. 75(1), pp. 1 –21 (2026)

DOI 10.24425/aee.2026.156799

Vibration influence and structural optimization analysis of rigid catenary in tunnel

XIA ZHAO [1], XUANCHENG WEI [1]✉, YING WANG [1], XIUQING MU [1], ZHULIN ZHANG [1], AIPING MA [2]

[1] *School of Automation and Electrical Engineering, Lanzhou Jiaotong University*
No. 88, Anning West Road, Lanzhou, People's Republic of China

[2] *China Railway Lanzhou Group Co., Ltd.*
China

e-mail: {2314486731/✉ 1010918476}@qq.com,

(Received: 11.07.2025, revised: 23.01.2026)

Abstract: With the continuous development of railway systems in China, the speed grades of trains have been consistently elevated, and the electrification of railways has become increasingly widespread. Consequently, higher requirements have been placed on the safety of electrified railway operations. However, during actual operation, pantograph-catenary failures occur frequently, disrupting current collection and affecting normal train operation. Particularly in the case of newly constructed tunnels employing rigid catenary systems, it is essential to consider the impact of pantograph-catenary dynamic interactions on cantilever-type supporting devices. Through finite element analysis of the cantilever assembly, the regions of maximum stress and strain, as well as areas susceptible to fatigue, were identified. Vibration characteristics and modal analysis were also conducted. The results indicate that fatigue-prone failure points in the rigid catenary system are primarily concentrated at the elastic clamps and rotating base. By reinforcing the material of these components to achieve sufficient strength and increasing the vibration frequency, the torsional vibration mode of the cantilever assembly was significantly improved. Furthermore, the addition of a leaf spring structure to the clamp assembly demonstrated excellent shock absorption and energy dissipation effects, thereby further enhancing the stability of the reinforced components.

Key words: catenary reliability, electrified railway, modal analysis, rigid catenary, vibration characteristics

1. Introduction

In recent years, rigid catenary is more and more commonly used in new long tunnels, especially in high plateau and high altitude areas, due to the harsh climate environment, resulting in frequent pantograph-catenary accidents. Particularly, the resonance effects caused by trains passing by,

and the ice accumulation effects on contact wires in extremely cold weather [1], have become key research topics in mitigating these impacts and enhancing the stability of the catenary system. Besides, rigid catenary has the characteristics of high hardness and high strength, can be maintenance-free, and is widely used in long tunnels and subway tunnels. When the train enters the tunnel at high speed, the surrounding space will be squeezed, the viscosity and compressibility of the air itself will cause great fluctuations in the squeezed air, and the movement of the surrounding flow field will be driven during the operation, forming a strong piston wind. The generated flow field will have a strong impact on the rigid catenary and its supporting devices can increase the load. The rigid catenary and its supporting devices are the most important components, which bear the common load of the pantograph and train piston wind. When the shock and vibration caused by the pantograph slide along with the action of piston wind, when these frequency of vibration reach the natural frequency of the rigid catenary and its arm device, great resonance phenomenon will occur to it, which will reduce the reliability of the rigid catenary and its arm device [2], at the same time, it increases the risk to the smooth operation of the railway. Therefore, it is necessary to analyze the vibration generated by the pantograph and to optimize the structure.

Modal analysis can be used for vibration studies, which analyzes the mode shape and resonance properties at the natural frequency of a vibrating structure, and provides a theoretical basis for its structural optimization. Pencody *et al*. [3] presented the modal analysis of the pavement slabs of different thicknesses, and the vibration characteristics of the airport pavement slabs with different thicknesses, to reduce the damage of the rigid pavement of the airport. Based on the influence of contact line galloping, reference [4] shows that after the installation of spacer-type anti-galloping devices, the main frequency of the conductor increases, thereby enhancing the current collection stability of the pantograph-catenary system. Ma Qiming *et al*. [5] carried out the modal analysis of the flexible catenary wrist arm based on ANSYS simulation. The resonance and other problems in the process of the pantograph taking current from the flexible catenary were also analyzed to improve the installation of flat and oblique wrist arms, and optimize the natural frequency of the contact suspension to improve the operation safety. Liu Xinlong *et al*. [6] based on the current-carrying wear test of rigid catenary, concluded that properly reducing the center distance of the contact line is beneficial to reduce the abnormal wear of the rigid catenary anchored joint part. In Sun Mengmeng *et al*.'s research [7], the vibration signals of the building structure are measured experimentally, and variational mode decomposition is applied to obtain single-modal signals. Then, the natural frequency and damping ratio of the structure are determined through iterative optimization. In Montserrat Simarro *et al*.'s research [8], the wear of the pantograph was determined by analyzing the variable parameters between the pantograph and the rigid catenary, as well as the proper assembly position of the rigid catenary. Feng Xiaohe *et al*. [9] based his research on the traditional rigid catenary busbar; six new types of busbars with high moment of inertia were developed. The static and dynamic performance of these new busbars was analyzed, demonstrating that this approach can effectively enhance the stability of both the rigid catenary busbar and the contact wire. Reference [10] indicates that variations in both wind speed and wind angle can cause wind-induced vibration in the contact line, and an increase in wind speed may lead to instability in current collection. Zhang Yangyang [11] used the ANSYS finite element analysis method to carry out static analysis and modal analysis of the rigid catenary. The resonant frequency and mode shape were obtained. The rationality of the data was proved by combining the measured data of the subway, which provided a basis for improving the stability of the pantograph-catenary relationship in the future.

This paper takes the rigid contact line inside a tunnel as the research object, analyzing the vibration impact of the pantograph on the contact line in railway tunnels. It conducts dynamic-static analysis and modal analysis on the vibration patterns and modal characteristics of the contact line system when trains pass through. By modifying the material thickness of the cantilever assembly and introducing a new geometric design for the clamp section of the cantilever assembly, a series of optimization measures is implemented to enhance the stability of the contact line system. The study provides references and a theoretical basis for the construction of contact line systems in subsequent long-span tunnels. Compared to existing literature, most studies focus on resolving issues through active control of the pantograph, with few considering optimization of the contact line assembly itself. The material modifications and geometric designs proposed in this paper represent a novel approach, and similar designs have not been encountered in related research to date.

2. Finite element analysis of rigid catenary

2.1. Rigid catenary and its supporting device structure

Compared to flexible catenary systems, the rigid catenary system inside tunnels is composed only of vertical supports, movable bases, anchoring components, insulators, rigid clamps, and a rigid busbar (typically configured as a hard crossbeam), along with some minor connecting elements [12]. A schematic diagram of this system and its components, photographed during an investigation of the Wushaoling Tunnel, is shown in Fig. 1.

In the finite element analysis of the rigid catenary, it is necessary to keep the meshing accurate and avoid the phenomenon of segmentation failure, and the model needs to be simplified when constructing the model, so that an intuitive model is obtained for analysis, and the simplified three-dimensional model is shown in Fig. 2.

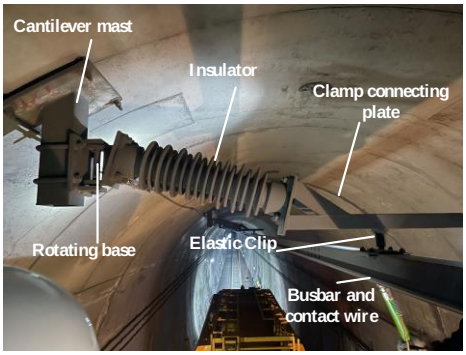

Fig. 1. Schematic diagram of the research system

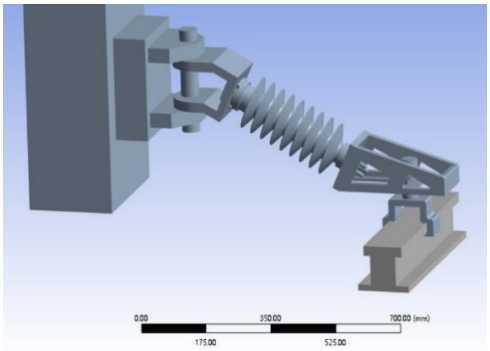

Fig. 2. Simplified rigid catenary support device

Due to the significant computational load involved in finite element analysis, and considering the practical implications of the results, components that can be temporarily added based on site conditions (such as shims) are omitted. Features with minimal impact on the study object, such as non-connecting holes, chamfers, and fillets, are also disregarded. Additionally, bolts at connection points and elastic clamp sections are simplified. These simplifications do not compromise the accuracy of the results while enabling rapid computation of the overall system response.

2.2. Meshing of rigid catenary wrist arms

When conducting static, modal, and dynamic analyses on the rigid catenary system and its cantilever assembly, solid element types are used for meshing. For components with regular shapes and simple structures, a larger mesh size (2.100006 mm) can be employed, though smaller sizes may also be used for calculation. For more complex components or those with significant bending deflection, a finer mesh size (0.999932 mm) is adopted. After meshing, the final model consists of 2 046 309 nodes and 901 385 elements. The meshed model of the rigid catenary system and its cantilever assembly is shown in Fig. 3.

The boundary conditions for the rigid catenary support assembly are set at the mast location of the cantilever. The fixed support of the catenary system is positioned at the top of the mast, aligning with actual on-site installation conditions. The fixed support is illustrated in Fig. 4. The cantilever assembly is constrained laterally by the mast, with the actual constraints comprising bolt pre-tension force, contact friction, structural stiffness, and installation clearance. The actual constraint characteristics provide limited bending stiffness while allowing slight rotation. In practical installation, the mast is also connected to embedded parts in the tunnel vault, consistent with the established boundary conditions.

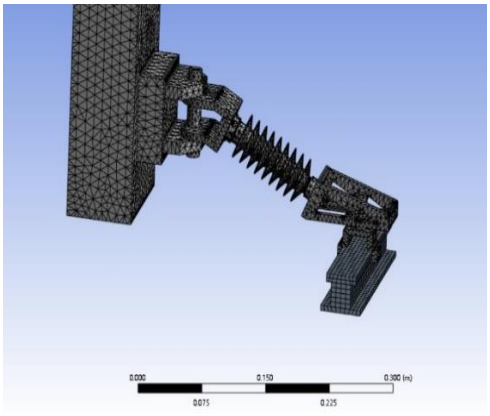

Fig. 3. Meshing of the rigid catenary and its wrist arm

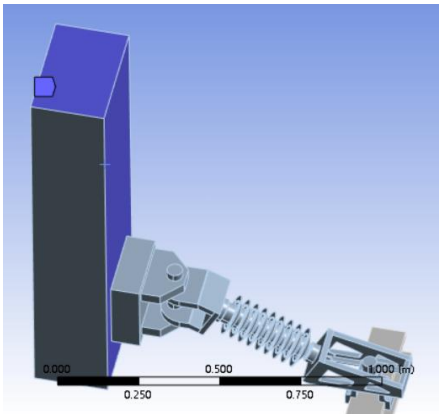

Fig. 4. Boundary conditions of rigid catenary

2.3. Mesh independence study and sensitivity analysis

To ensure the accuracy of simulation results without being unduly influenced by discretization errors, a mesh convergence study was conducted using the output equivalent stress as the evaluation metric.

In the global model, a sequence of progressively refined mesh schemes was defined with element sizes of 2.5 mm, 1.5 mm, 1.0 mm (currently selected), and 0.7 mm. While keeping the loading, boundary conditions, and all other settings constant, only the mesh density was varied across multiple simulations. The computational results are summarized in Table 1.

Table 1. Mesh computational results

Mesh scheme	Mesh size (mm)	Number of nodes	Number of units	Maximum equivalent stress (MPa)	Maximum displacement (mm)	Calculate time (s)
Coarse mesh	2.1	18 565	13 100	60.971	0.318	26
Medium mesh	1.5	65 832	71 500	83.373	0.371	45
Fine mesh	1.0	2 046 309	901 385	95.849	0.436	180
Finest mesh	0.7	3 969 873	1 510 723	103.37	0.460	3 600

Meanwhile, the relative error and convergence of the computational mesh are evaluated. Using the results from the finest mesh as the reference value, the relative errors of the results from coarser meshes are calculated.

$$\text{Relative Error}\,(e_i) = \left|\frac{S_i - S_{\text{ref}}}{S_{\text{ref}}}\right| \times 100\%, \tag{1}$$

where S_i represents the result of the i-th mesh scheme (stress value), and S_{ref} denotes the result of the finest mesh scheme.

It can be obtained that the stress error of the medium mesh is

$$(1.5\text{ mm}) = 83.373 - 103.37|/103.37 \times 100\% \approx 19.3\%.$$

The stress error of the fine mesh is

$$(1.0\text{ mm}) = 95.849 - 103.37|/103.37 \times 100\% \approx 7.3\%.$$

The results indicate that when the element size is refined below 1.0 mm, the change in maximum equivalent stress significantly slows down. Using the results of the finest mesh (0.7 mm) as a reference, the stress error of the fine mesh with an element size of 1.0 mm is only 7.3%, while the computation time is merely 1/20 of that required for the finest mesh.

Therefore, considering both computational accuracy and efficiency, this study adopts the fine mesh scheme (element size 1.0 mm, approximately 901 385 elements) for all subsequent analyses. The results obtained with this scheme can be considered mesh-independent.

2.4. Rigid catenary materials and pantograph-catenary dynamic parameters

The most commonly used material for the rigid catenary system is carbon structural steel, and there are two types of it: Q235B and Q345B. Q345B has better strength and toughness than Q235B, and Q345B is more suitable for the study of its vibration characteristics in this paper. The catenary clip and the base are connected by insulators, and the insulators are mostly made of ceramic or hard rubber. The insulators have little influence on the overall during the vibration analysis and modal analysis of the overall device, which can be ignored. In summary, the rigid catenary and its wrist arm materials are shown in Table 2.

Table 2. Material parameters

Parameter	Quantity
Young's modulus	124 000 MPa
Tensile strength	358 MPa
Vibrational quantity	2×10^6 times
Busbar weight	5.9 kg/m
Density	7.85×10^3 kg/m^3
Moment of inertia	1×10^{-6} m4

This study is based on the rigid catenary system in the Wushaoling Tunnel of the Lanxin Railway. The tunnel has a speed limit of 120 km/h, and the pantograph selected for this study is the DSA200 model, which is capable of operating at speeds of up to 200 km/h. The operating parameters of this pantograph at 120 km/h are presented in Table 3.

Table 3. Parameters of DSA 200 pantograph

Parameter	Quantity
Average contact force/N	81.9
Maximum contact force/N	119.89
Maximum lifting height/mm	3 000
Minimum contact force/N	57.47
Natural frequency/Hz	20.557

2.5. Static structural analysis

When the rolling stock is stationary on the track or moving at a constant speed (under absolute conditions), the rigid catenary and its cantilever assembly are subjected to a static contact force applied by the pantograph. Meanwhile, due to the varying connection methods within the catenary system, the transmission of the pantograph's static contact force results in different constraints and deformations across the components.

The overall rigid catenary system inside the tunnel consists of a cantilever post, rotating base, anchor bolts, insulators, clamp connecting plates, elastic clamps, a busbar, and a contact wire [12]. When the pantograph slider exerts an upward force on the contact wire, the force is transmitted through the elastic clamp to the clamp connecting plate, then to the insulator, and finally to the rotating base, which is connected to the post. The post provides fixed support for the entire cantilever assembly. In the static analysis, a fixed support is applied to the post connection surface, the static uplift force of the pantograph is applied to the bottom of the rigid catenary, and gravitational acceleration is applied to the cantilever assembly.

Under actual conditions, the static uplift force of the pantograph is typically around 120 N [13]. The static analysis reveals that the maximum stress under this condition is approximately 95.849 MPa, primarily located at the connection between the insulator and the rotating base. This stress concentration occurs because the pantograph's uplift force is transmitted through the elastic clamp connecting plate to the insulator and the rotating base, making this area particularly stressed, as shown in Fig. 5. The rigid catenary cantilever structure can be equivalently modeled as a cantilever beam, with one end fixed to the post via the rotating base and the other end supporting the rigid catenary beam in a suspended arrangement. The free end of the cantilever beam is analogous to the suspended end of the structure, which is most prone to deformation under load, exhibiting the largest displacement. Accordingly, the maximum deformation in the static analysis occurs at the rigid catenary beam and the elastic clamp connecting plate, with a displacement of 0.43639 mm, as illustrated in Fig. 6. This deformation falls within the design requirements, confirming the structural adequacy of the catenary system.

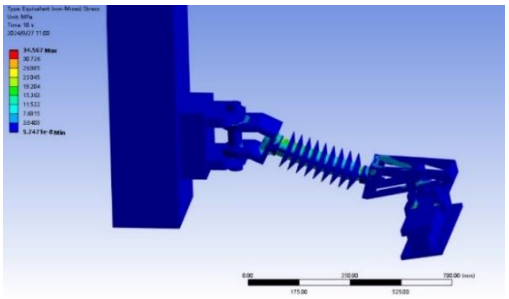

Fig. 5. Stress-load diagram under static analysis

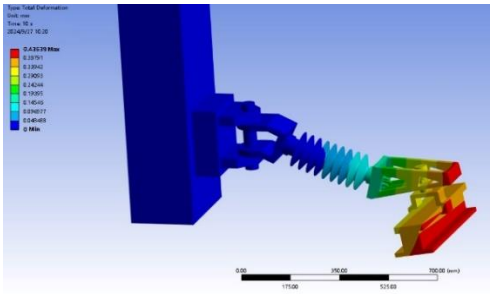

Fig. 6. Total deformation under static analysis

2.6. Dynamic structural analysis

Dynamic load analysis involves applying loads that vary over time. Under dynamic contact conditions at speeds not exceeding 250 km/h, the maximum contact force should not exceed 250 N, the minimum contact force should not be less than zero, and the average contact force should not exceed 130 N [13]. Under these conditions, the maximum stress is approximately 118.21 MPa, with stress concentrations still primarily located at the insulator and rotating base.

Compared to static analysis, dynamic analysis involves varying stress and total deformation at each time step. These variations can generally be represented using time functions or harmonic signals. This condition reflects the scenario when a locomotive pantograph dynamically traverses the rigid catenary system, applying random dynamic loads from the pantograph's uplift force to the cantilever support assembly. This force is applied to the surface of the rigid catenary.

The dynamic load analysis reveals that the maximum stress, elastic strain, and total deformation of the rigid catenary and its support assembly are greater than those under static loads. Additionally, the load values vary at different time steps, exhibiting greater randomness compared to static loads. However, the critical load-bearing areas remain concentrated at the insulator and clamp connecting components. The maximum stress and total deformation are shown in Fig. 7 and Fig. 8.

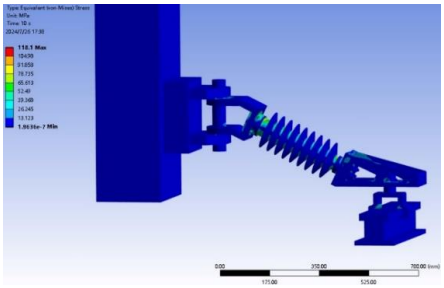

Fig. 7. Equivalent stress under dynamic load

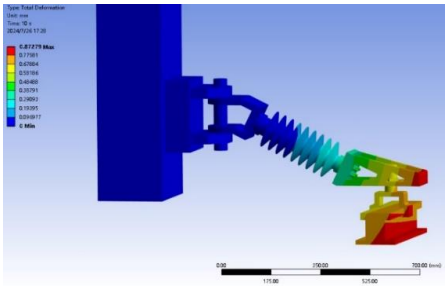

Fig. 8. Total deformation under dynamic load

3. Theoretical analysis of rigid catenary

3.1. Initial deflection and stress calculation analysis

Based on its structural characteristics, the system can be equivalently modeled as a cantilever beam structure with a concentrated mass and a concentrated force applied at one end. A schematic cross-sectional view illustrating the principle of the pantograph uplift force acting on the rigid catenary and its support assembly is shown in Fig. 9.

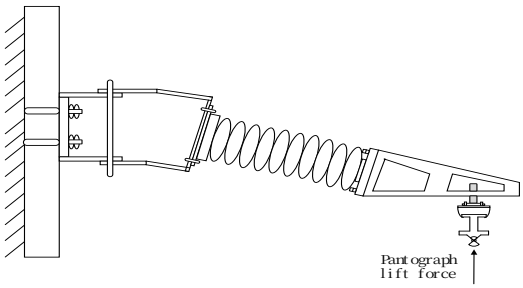

Fig. 9. Cross-sectional view of the force principle

The schematic diagram of the coordinate system can be simplified for easy calculation, and the simplified schematic diagram is shown in Fig. 10.

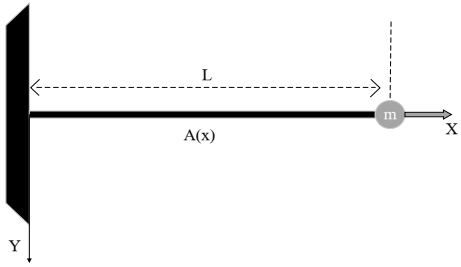

Fig. 10. Cross-sectional of the simplified principle

According to the simplified schematic diagram, the equivalent mass can be solved, and the corresponding coordinate system can be established firstly, and the bending moment equation can be obtained:

$$m\left(x\right) = -F\left(l - x\right). \tag{2}$$

Differential equations for deflection curves of beams:

$$m\left(x\right) = -EIw''(x), \tag{3}$$

where EI represents the bending stiffness of the beam and $w''(x)$ represents the curvature of the beam, which can be obtained by combining the above formulas:

$$F(l - x) = EIw''(x). \tag{4}$$

Using twice the integral method, one can get:

$$Cx + D + F\left(\frac{l}{2}x^2 - \frac{1}{6}x^3\right) = EIw(x). \tag{5}$$

When the rotation angle of the rigid catenary and its cantilever device at the fixed end is 0 (horizontal position), the deflection at this time is also 0 and corresponding to the equation, that is, $x = 0 \rightarrow w\left(x\right) = 0, w'\left(x\right) = 0$. Bringing this resolution into Eqs. (4) and (5), $C = 0$ and $D = 0$ can be obtained, then importing the result into Eq. (5) yields the following:

$$w\left(x\right) = \frac{F}{EI}\left(\frac{l}{2}x^2 - \frac{1}{6}x^3\right). \tag{6}$$

Similarly, let $y_{\max}$ be the distance from the neutral axis of the cross-section to the outermost edge. The maximum normal stress in the beam during bending can be expressed by the bending formula as $\delta_{\max} = \dfrac{y_{\max} m\left(x\right)}{I}$. Substituting the bending moment equation $m(x)$ from Eq. (2) into this, we obtain:

$$\delta_{\max} = \frac{y_{\max} FL}{I}. \tag{7}$$

If a section of the rigid cantilever beam with a length of $L = 2$ m is considered, and a concentrated force of $F = 1$ kN is applied to the cantilever beam, the maximum stress calculated using Formula (7) yields $\delta_{\max} = 100$ MPa. This value is essentially consistent with the static maximum stress of 95.845 MPa obtained from the simulation experiment, thereby validating the theoretical simulation as fundamentally correct. Moreover, the selected parameters align well with actual field conditions.

3.2. Post-equivalence quality analysis

In the equivalent analysis of the whole system, the equivalent mass of the rigid catenary at the free-end of the cantilever beam is m_{eq}, the concentrated mass of the model is also at the free-end, and the bending deflection of the model is greatest when the free-end of the cantilever is dynamically lifted by the pantograph and $x = l$, as shown in Fig. 11.

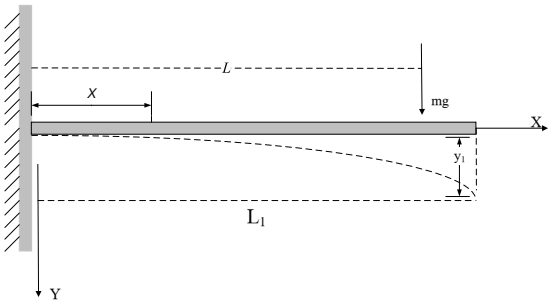

Fig. 11. Section view of cantilever after stress bending

The maximum displacement set is $w_{\max} = \dfrac{Fl^3}{3EI}$. Since $F = mg$, $w_{\max} = \dfrac{mgl^3}{3EI}$. We obtained:

$$mg = \frac{3EI}{l^3} w_{\max}(x). \tag{8}$$

Bringing Eq. (8) into Eq. (6) yields:

$$w\,(x) = w_{\max}\left(\frac{3x^2}{2l^2} - \frac{x^3}{2l^3}\right). \tag{9}$$

In the impact state, the dynamic response of the cantilever beam can be calculated by the energy method, and when the object acts on the cantilever beam with a certain impact force, the dynamic response of the cantilever beam can be simulated and analyzed by the law of conservation of kinetic energy. The maximum kinetic energy is set as T_m:

$$T_m = \frac{1}{2}\int_0^l A(x)\rho\left(\frac{\mathrm{d}w}{\mathrm{d}t}\right)_m^2 \mathrm{d}x, \tag{10}$$

where ρ represents the unit volume mass of the beam, and because

$$\left(\frac{\mathrm{d}w}{\mathrm{d}t}\right)_{\max} = \left(\frac{\mathrm{d}w_m}{\mathrm{d}t}\right)_{\max}\left(\frac{3x^2}{2l^2} - \frac{x^3}{2l^3}\right).$$

Bringing this equation into Eq. (9) yields:

$$T_m = \frac{1}{2}\int_0^l A(x)\rho\left(\frac{\mathrm{d}w_m}{\mathrm{d}t}\right)^2\left(\frac{3x^2}{2l^2} - \frac{x^3}{2l^3}\right)\mathrm{d}x. \tag{11}$$

When the equivalent mass m_{eq} is present, the maximum kinetic energy after equivalent is:

$$T_m = \frac{1}{2}m_{eq}\left(\frac{\mathrm{d}w_m}{\mathrm{d}t}\right)^2. \tag{12}$$

Dividing Eq. (11) by Eq. (12) yields:

$$m_{eq} = \int_0^l A(x)\rho \left(\frac{3x^2}{2l^2} - \frac{x^3}{2l^3}\right)^2 \mathrm{d}x, \tag{13}$$

where $A\,(x)$ in all of the above equations is the cross-sectional area of the beam, and when $A\,(x)$ is a linear function, the equivalent mass is:

$$m_{eq} = \rho \int_0^l (ax+b)\left(\frac{3x^2 l - x^3}{2l^3}\right)\mathrm{d}x = \frac{\rho}{4l^6}\int_0^l (ax+b)(9x^4l^2 + x^9 - 6x^5 l)\mathrm{d}x,$$

$$m_{eq} = \left(\frac{43}{224}al + \frac{33}{140}b\right)\rho l. \tag{14}$$

When $A\,(x)$ is constant, that is, when $A\,(x) = a$, the equivalent mass is:

$$m_{eq} = \frac{33}{140}\rho l a. \tag{15}$$

Based on the review of relevant materials [14] and in combination with the actual working conditions on site, by substituting them into Eq. (14) or Eq. (15), the equivalent mass m_{eq} can be obtained as approximately 27.3 kilograms.

Equivalent mass is not a simple sum of all individual masses; it represents the total inertia exhibited by the system when motion occurs in the vertical direction (at the contact point). It is a mass in the "dynamic sense."

Simultaneously, it reflects the degree of mass participation. When the pantograph lifts the contact line, it does not need to raise the entire infinitely long contact wire, but primarily excites vibrations in a localized region of the conductor. The equivalent mass quantitatively describes the magnitude of the "effective mass" participating in this localized vibration. The coefficient α indicates how much of the contact line's mass is involved in the motion.

3.3. Equivalent stiffness analysis

As shown in Fig. 11, when the load on the cantilever beam is mg, it is assumed that the longitudinal displacement of y_1 is generated:

$$y_1 = \frac{mgL^3}{3EI}. \tag{16}$$

And because the equivalent stiffness of the entire cantilever beam structure is the generalized force at the loading point divided by the generalized

$$k'_{eq} = \frac{mg}{\frac{mgl^3}{3EI}} = \frac{3EI}{l^3}. \tag{17}$$

The pantograph and the rigid catenary system can be equivalent to the elastic model, and the pantograph is equivalent to the spring with stiffness k_c. Since the equivalent mass m_{eq} of the

free-end of the equivalent rear beam is consistent with the displacement direction of the pantograph lifting of the locomotive, the pantograph stiffness k_c and k'_{eq} are superimposed together to obtain the final overall equivalent stiffness:

$$k_{eq} = \frac{k'_{eq} k_c}{k'_{eq} + k_c}. \tag{18}$$

Based on the review of relevant materials [14] as well as the actual working condition values on site and substituting them into Eq. (18), it can be concluded that the simplified equivalent elastic stiffness k_{eq} is approximately $6.9{\times}10^7$N/m. According to the above reasoning, the stiffness equivalent model can be made as shown in Fig. 12.

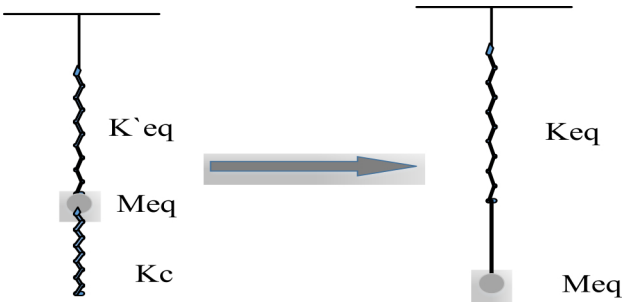

Fig. 12. Stiffness equivalent of free-end of rigid catenary

The equivalent stiffness k_{eq} represents the structure's ability to resist static deformation or dynamic displacement. Physically, it characterizes the comprehensive resistance to deformation of the entire catenary system by an "equivalent spring" stiffness. In other words, it reflects the total elastic restoring force generated by the system when the pantograph lifts the contact line by a unit height.

The equivalent stiffness primarily stems from two sources: first, the pantograph stiffness k_c, where the lifting device acts like a spring attempting to push the sliding plate upward; second, the stiffness of the rigid catenary, which mainly arises from the bending stiffness of the conductor, rather than the tension as in flexible catenary systems. This is one of the most fundamental distinctions between rigid and flexible catenary systems.

3.4. Fatigue life analysis

The catenary support assembly is subjected to fluctuating stresses at certain points due to variations in the pantograph uplift force. After a sufficient number of cyclic loadings, cracks may initiate or complete fracture may occur, indicating fatigue failure in the support assembly. The number of cyclic loadings is generally denoted as N. Currently, a widely used fatigue analysis method is the stress-based S-N approach. As long as the material properties, stress conditions, and loading spectrum remain identical, the fatigue life does not vary with changes in the specific structural form.

For a known relationship between material properties, applied stress, and fatigue life (S-N method), the correlation between power density and fatigue life for the studied object can be

derived. Its mathematical expression is as follows:

$$\frac{\mathrm{d}S}{\mathrm{d}t} = f1(N_f), \tag{19}$$

where $\mathrm{d}S/\mathrm{d}t$ represents the power density of the load signal and N_f denotes the limiting number of cycles for fatigue failure of the studied object.

For the signals to be studied in this paper, which are generally broadband signals, there should be a corresponding power density at each time instant. Using the short-time Fourier transform (STFT), these signals can be decomposed into a sum of multiple cosine functions with different dominant frequencies. The mathematical expression is shown in Eq. (20):

$$\left(\frac{\mathrm{d}S}{\mathrm{d}t}\right)_{t=t_0} = \sum_i A_i \cos\left(F_i \Delta t\right), \tag{20}$$

where F_i represents the dominant frequencies at different time instances obtained through the short-time Fourier transform, and the corresponding power density value is:

$$A_i = \left(\mathrm{d}S/\mathrm{d}t\right)_{t=t_0,i} \tag{21}$$

According to fatigue damage theory, when $t = t_0$ the damage rate within the adjacent time interval Δt caused by the power density at that time can be expressed mathematically as:

$$D = \sum_i N_i/\left(N_f\right)_i, \tag{22}$$

where the fatigue damage rate within the time interval Δt is denoted by D.

$$N_i = F_i \Delta t, \tag{23}$$

where: F_i denotes the dominant frequency, Δt represents the time interval at $t = t_0$, and N_i indicates the total number of cycles within this time interval.

$$\left(N_f\right)_i = f2\left[\left(\mathrm{d}S/\mathrm{d}t\right)_{t=t_{0,i}}\right], \tag{24}$$

where $\left(N_f\right)_i$ represents the total number of cycles until fatigue failure occurs in the material of the studied object.

Given a total of m time steps, the cumulative fatigue damage generated within this range can be expressed as:

$$AD = \sum_{j=1}^{m}\left(\sum_i N_{j,i}/\left(N_f\right)_{j,i}\right), \tag{25}$$

where j denotes the time step index, $j = 1, 2, \ldots m$, and AD represents the cumulative damage generated during this period. Accordingly, the criterion for fatigue failure of the studied material is defined as:

$$AD = \sum_{j=1}^{m}\left(\sum_i N_{j,i}/\left(N_f\right)_{j,i}\right) \geq 1. \tag{26}$$

Therefore, based on fatigue damage theory, if the material of the studied object accumulates a fatigue damage of AD within a given time period T, its fatigue life can be estimated as follows:

$$LF = \frac{T}{AD}, \tag{27}$$

where T represents the duration of the load acting on the studied object, in seconds (s). LF denotes the estimated fatigue life of the material of the studied object, in seconds (s).

4. Integral modal analysis of rigid catenary system

According to the simulation results presented in Section 1, the fatigue-prone areas of the rigid catenary system and its support assembly are located at: the busbar of the catenary and the elastic clamp section; the riveted connection between the elastic clamp connector and the insulator; and the riveted connection between the insulator and the rotating base of the cantilever.

By performing a modal analysis of the assembly, the natural frequencies are examined to identify regions susceptible to resonance. Based on this, optimization measures are proposed to address vibration-related issues.

4.1. Theoretical analysis

The vibration of the unit beam structure can be expressed by the differential equation:

$$Mx'' + \zeta x'' + Kx - F = 0. \tag{28}$$

The mass matrix of the vibration system can be expressed by M, the damping matrix is ζ, K is the stiffness matrix, F is the external force, and x is the displacement of the structure under the applied force.

In the modal analysis, different modes will correspond to different vibration frequencies, so that the above equation $F = 0$, and when there is no external force, the catenary device works under-damping conditions, corresponding to the formula $\zeta = 0$. The differential equation under the underdamping condition can be obtained:

$$Mx'' + Kx = 0. \tag{29}$$

By the solution of differential equations, the general form of the solution of Eq. (29) is

$$x = \varphi e^{i\omega t}. \tag{30}$$

Bringing Eq. (30) into Eq. (29) gives the solution to the vibration equation of the device:

$$K\varphi = \lambda M\varphi, \tag{31}$$

where: φ is the eigenvector of the system, and its corresponding eigenvalues λ, i represents the imaginary units, ω is the natural frequency of the vibrating device, and t is the vibration time. According to Liang Jun's research [15] in the theoretical analysis of working modes, it can be seen that when $\lambda = \omega^2$, the eigenvalues in the modal analysis can be obtained. λ_i denotes the i-th order eigenvalue and also the intrinsic frequency $\omega_i = \sqrt{\lambda_i}$, and φ_i denotes the eigenvector at the i-th order, which corresponds to the structural deformation in the i-th mode shape in the vibration model.

4.2. Analysis of results

For mechanical structures, different modes correspond to distinct modal shapes. Lower-order modes generally have a greater impact on the dynamic performance of the structure, as they represent the most fundamental vibration patterns of the structure [16]. In contrast, higher-order modes typically exhibit vibration frequencies greater than the natural frequency, with rapid amplitude decay, making them less likely to cause resonance-induced structural damage [17]. For an intuitive analysis, the first four vibration frequencies or modal shapes can be extracted. The deformation magnitudes of the extracted first four modal shapes are shown in Fig. 13, with the measurement point locations referenced from the actual maintenance practices of the rigid catenary system in the tunnel located in the western plateau region, as illustrated in Fig. 14.

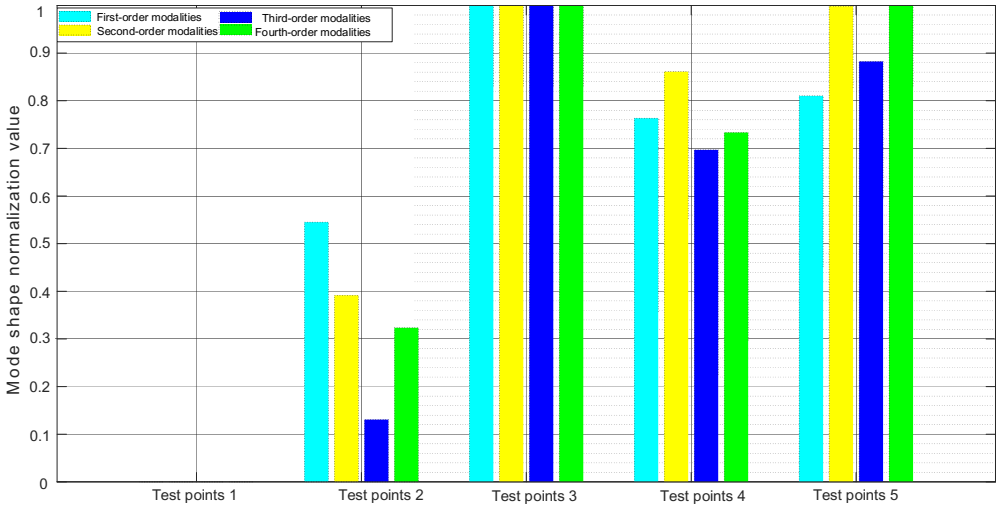

Fig. 13. Normalized value of the total deformation of vibration modes

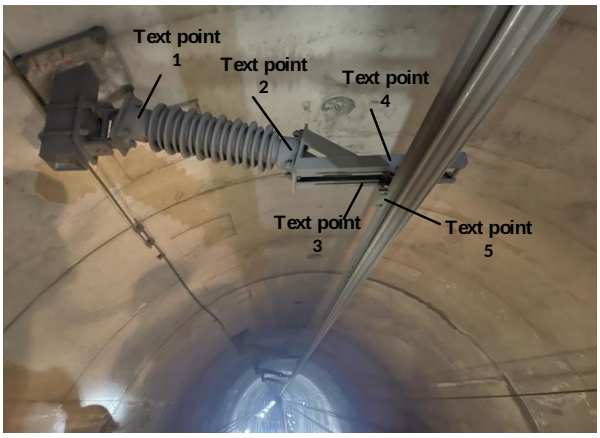

Fig. 14. Actual position of vibration mode measurement point

The first-order modal shape of the rigid catenary system is primarily characterized by torsional vibration. When the locomotive pantograph moves along the contact wire, uneven force distribution – caused by changes in the catenary stagger or when the train passes through curved sections – can induce torsion in the rigid catenary. This phenomenon may lead to insulator fracture or clamp displacement, resulting in pantograph-catenary faults, as illustrated in Fig. 15. The third to fifth-order modal shapes are predominantly characterized by first-order bending vibration.

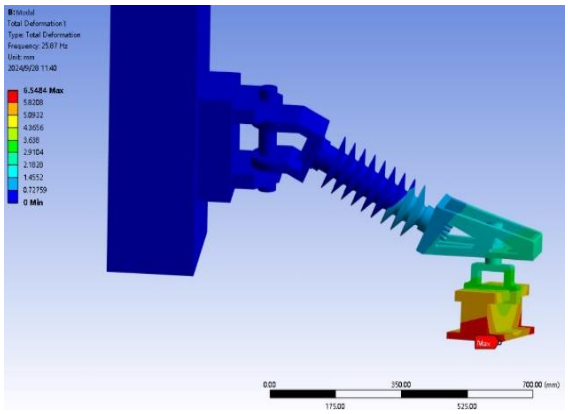

Fig. 15. Total deformation under first order mode shape

Analysis of the first six low-order modal shapes reveals that their natural frequencies range from 23.87 Hz to 364.39 Hz, with each mode exhibiting either torsional or bending vibrations. According to the ANSYS modal analysis, the first torsional mode occurs at 23.87 Hz, and the first bending mode appears at 71.978 Hz. These two modal shapes constitute the primary low-order vibration modes of the system and have a significant impact on pantograph-catenary interaction failures.

According to relevant literature, when a conventional pantograph slider moves along the contact line as a rigid body, the excitation frequency between the pantograph and the catenary is typically around 20 Hz [19]. The current un-optimized first and second natural frequencies are found to be 23.87 Hz and 31.1 Hz, respectively, which are close to the 20 Hz excitation frequency. This proximity increases the risk of resonance and therefore requires modification.

The first-six modes of the rigid contact line system are shown in Table 4.

Table 4. The first six natural frequencies of the rigid catenary system

Modal order	**Natural frequency/Hz**
1	23.87
2	31.1
3	50.437
4	71.978
5	139.29
6	264.39

5. Design and optimization of rigid catenary system

5.1. Optimization idea

(I) Based on the results of stress fatigue analysis and modal analysis, to reduce resonance induced by low-order modes, the material strength can be appropriately increased or the structure can be reinforced by adding material thickness. This method can appropriately increase the first-order torsional frequency [18]. However, compared to flexible catenary systems, the rigid catenary uses Q345B structural steel, which already meets the required material stiffness. Therefore, only an appropriate increase in material thickness is needed to achieve a more stable state. A comparison of the assembly before and after optimization is shown in Fig. 16.

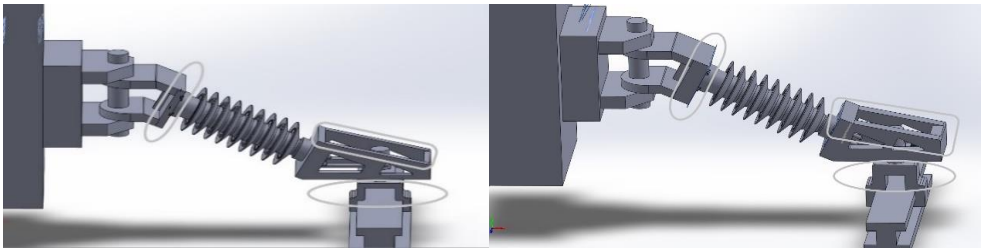

Fig. 16. Comparison of device before and after thicken

By appropriately adjusting the thickness of the rigid catenary clamp connecting plate (measurement point 3), the corresponding changes in vibration frequency under different modes caused by thickness variations can be obtained, as shown in Fig. 17.

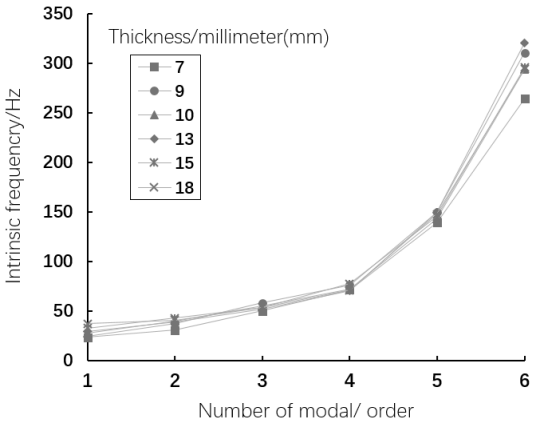

Fig. 17. Vibration frequencies for different thicknesses

As shown in Fig. 17, when the thickness of the base of the elastic clamp connecting plate increases from 7 mm to 18 mm, the modal frequencies also continuously rise. The changes in the 1st to 3rd order frequencies are relatively small, while the changes in the 4th to 6th order frequencies

are more significant. This verifies that modifying the material thickness can optimize the vibration frequencies of the system. Selecting an appropriate material thickness helps reduce the likelihood of resonance and improves the stability of the system under actual working conditions.

(II) On the basis of structural reinforcement, a Π-shaped leaf spring is installed above the clamp. It is an elastic leaf spring structure, as shown in Fig. 18. The leaf spring structure offers excellent damping and self-resetting capabilities. When the pantograph passes through, it lifts the busbar, which then comes into contact with the spring. This mechanism helps cushion the impact from the pantograph and enhances the elasticity of the transition section. Such a device has not been used in rigid catenary systems domestically or internationally, making it a novel solution.

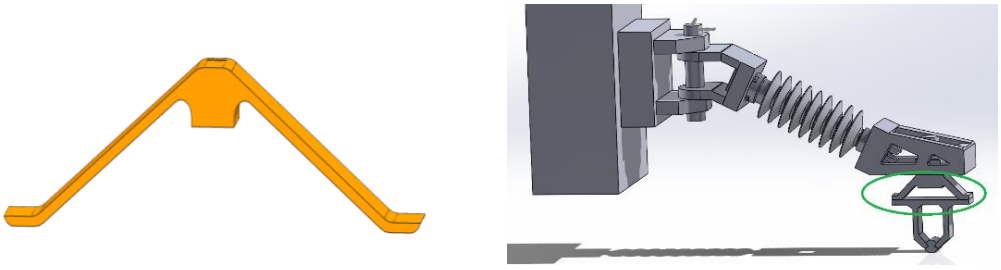

(a) (b)

Fig. 18. Schematic diagram of the structure after optimizing the spring leaf

5.2. Optimized results

(I) After structural optimization, a modal analysis was conducted again, and the new six-order modal frequencies are shown in Table 5. It can be observed that when the reinforcement thickness reaches 13 mm, the low-order modes are effectively controlled post-optimization. The first-order modal frequency increases from 23.87 Hz to 31.02 Hz, and the third-order modal frequency rises from 50.437 Hz to 52.638 Hz. This improvement moderately enhances the vibration frequency characteristics of the system and optimizes the overall dynamic performance of the assembly.

Table 5. The first-sixth natural frequencies of the optimized system

Modal order	Natural frequency/Hz
1	31.02
2	39.632
3	52.638
4	70.96
5	149.829
6	320.532

A comparison of frequencies before and after the modification shows that, after optimization through increased thickness, the frequencies are concentrated within the range of 31.02 Hz to 320.532 Hz. When a conventional pantograph slider moves along the contact line as a rigid body, the excitation frequency between the pantograph and the catenary is typically around 20 Hz [19]. The natural frequency of the optimized rigid catenary system now exceeds the vibration frequency induced by pantograph uplift. As a result, the impact of the pantograph on the overall catenary system is reduced, leading to more stable current collection during locomotive operation and a decreased probability of pantograph-catenary faults.

(II) Similarly, a modal analysis was performed on the assembly with the added leaf spring structure. Installing the leaf spring at the clamp connection area allows for better control of the vibration frequencies. The low-order modes are further improved compared to the reinforced-only structure. The resulting six-order modal frequencies are listed in Table 6. Specifically, the first-order modal frequency increases from 31.02 Hz (after reinforcement) to 60.594 Hz, and the third-order modal frequency rises from 52.638 Hz to 66.75 Hz. This further enhances the structural vibration characteristics beyond the initial reinforcement, leading to improved stability during train operation.

Table 6. The first sixth natural frequencies with leaf spring structure

Modal order	**Natural frequency/Hz**
1	60.594
2	62.716
3	66.75
4	160.613
5	236.83
6	380.93

A comparison shows that after the addition of the leaf spring structure, the frequencies are concentrated in the range of 60.594 Hz to 380.93 Hz. The low-order modal frequencies now exceed the maximum vibration frequency between the pantograph and the catenary [19]. As a result, the frequency generated by pantograph motion no longer coincides with the natural frequencies of the structure, reducing the likelihood of resonance. This improvement allows for better current collection during locomotive operation and provides significant support for progressively higher speed levels.

By comparing the mathematical model of the cantilever assembly with simulation results from the pre-optimized design, it is evident that the improved cantilever system exhibits notably enhanced bending resistance and vibration damping characteristics. Particularly after implementing the leaf spring support structure, the low-order natural frequencies are elevated, effectively avoiding resonance caused by frequency overlap. This enhancement significantly improves the stability of locomotive operation under high-speed conditions.

6. Conclusions

As the most widely used current collection system in long railway tunnels and urban rail transit today, the rigid catenary system can experience pantograph-catenary faults or even threaten normal train operation if any of its components are damaged. This study primarily conducts ANSYS finite element analysis on the rigid catenary system to examine its vibration behavior under static and dynamic contact forces, employing modal analysis to mitigate the impact of natural frequencies on the overall system. The optimized design of the cantilever assembly demonstrates both innovation and practicality, with key conclusions summarized as follows:

1. A finite element model of the rigid catenary system was constructed based on actual field conditions, revealing that fatigue-prone areas are most prominent at the connections between the insulator and the anchor base, the insulator and the elastic clamp connecting plate, and the elastic clamp and the contact wire beam.
2. Under real-world operational conditions, the dynamic uplift force exerted by the pantograph during motion has a slightly greater impact on the system compared to static conditions.
3. Modal analysis indicates that the system's vibrations are primarily characterized by first-order torsional and bending modes. The simulation results confirm that post-optimization; the system exhibits enhanced stability and reduced failure rates, validating the rationality of the improvements.
4. By incorporating modal theory, modal analysis of the rigid catenary system revealed that the first-order natural frequency closely approximates the dominant excitation frequency, posing a resonance risk. Increasing the thickness of the assembly raised the first-order torsional frequency from 23.87 Hz to 31.237 Hz, surpassing the dominant excitation frequency and altering the torsional and bending modes, thereby preventing pantograph-catenary faults and potential railway safety incidents.
5. The addition of a Π-shaped leaf spring to the clamp section of the rigid catenary cantilever assembly represents a highly innovative approach, as no similar studies have been reported in rigid catenary systems domestically or internationally. Simulation experiments demonstrate that this leaf spring structure further enhances the low-order modal frequencies compared to mere structural reinforcement, ensuring safer and more reliable current collection for locomotives. This advancement lays a solid foundation for future research on rigid catenary systems adapted for higher-speed applications.

Acknowledgements

Funded by the National Natural Science Foundation of China (Grant No. 52367009), the "Innovation Star" Project of Gansu Provincial Universities of China (No. 2025CXZX-661), the Lanzhou Bureau Group Corporation Science and Technology Research and Development Plan Project in China(No. LZ-YSZD-kyjsjds-jskfb-20250004), and the General Project of Gansu Provincial Science and Technology Research Program Joint in China (No. 25JRRA1167).

References

[1] Tian jingjing, Hu Liguo, Wang Ying, Zhao Feng, Chen Xiaoqiang, *Reliability prediction analysis of catenary after icing based on Kriging model*, Archives of Electrical Engineering, vol. 74, no. 1, pp. 1–16 (2025), DOI: 10.24425/aee.2025.153914.

[2] Zhuojun Li, Chunjiang Chen, Huapu Song, *Computational fluid dynamics-multibody system dynamics bidirectional coupling calculation and flow-induced vibration evaluation of a high-speed pantograph-catenary system*, Engineering Applications of Computational Fluid Mechanics, vol. 15, no. 1 (2025), DOI: 10.1080/19942060.2025.2512954.

[3] Peng Kedi, Zhao Hongduo, *Finite Element Model for Modal Analysis of Rigid Pavement and its verification*, Journal of Jilin University (in Chinese), vol. 1, no. 19 (2024).

[4] Zhang You Peng, Zhang Yahui, Zhao Shanpeng, *Effectiveness analysis of anti-galloping of spacer for catenary additional wires in strong wind section of high-speed railways*, Archives of Electrical Engineering, vol. 73, no. 2, pp. 499–517 (2024), DOI: 10.24425/aee.2024.149929.

[5] Ma Qiming, Wu Jiqin, Xie Dongxu, *Study on Stress Distribution of wrist Arm and Modal Characteristics of Contact Suspension*, Electrified Railway (in Chinese), vol. 33, no. 19 (2022).

[6] Liu Xinlong, Zhang Wulue, Xiao Qian, *Study on the effect of different structural parameters on the wear mechanism in the anchor-segment joint of the rigid overhead catenary*, Tribology International, vol. 191, no. 109108 (2024), DOI: 10.1016/J.TRIBOINT.2023.109108.

[7] Sun Mengmeng, Zhi Lunhai, *Modal parametric identification of building structures based on VMD*, Journal of Vibration and Shock (in Chinese), vol. 39, no. 1, pp. 175–183 (2020).

[8] Montserrat Simarro, Postigo S., Carlos Casanueva, *Influence of main operating conditions on contact wire wear of rigid catenary lines*, Tribology International, vol. 196, no. 109708 (2024), DOI: 10.1016/J.TRIBOINT.2024.109708.

[9] Feng Xiaohe, Gao Shibin, *Song Yang, Static and Dynamic Analysis of Conductor Rail with Large Cross-Sectional Moment of Inertia in Rigid Catenary Systems*, Energies, vol. 16, no. 1810 (2023), DOI: 10.3390/EN16041810.

[10] Yang Song, Zhigang Liu, Hongrui Wang, *Nonlinear analysis of wind-induced vibration of high-speed railway catenary and its influence on pantograph–catenary interaction*, Vehicle System Dynamics, vol. 54, no. 6, pp. 723–727 (2016), DOI: 10.1080/00423114.2016.1156134.

[11] Zhang Yangyang, *Research on Coupling Dynamic Simulation of Rigid Suspension Catenary*, Master's thesis, Faculty of Electrical Engineering, Southwest Jiao tong University, China (2012).

[12] He Guojun, *Research Progress and Prospect of 160 km/h Overhead Rigid Catenary* , Engineering construction and design (in Chinese), vol. 19, pp. 131–134 (2022).

[13] National Railway Administration of China, *High Speed Railway design code* [S], China Railway Press (2014).

[14] Zhang Hanbo, *Study on fatigue characteristics of AC25kV rigid catenary wrist arm support device*, Master's thesis, Faculty of Electrical Engineering, Southwest Jiao tong University, China (2019).

[15] Liang Jun, Zhao Dengfeng, *Research Status and Development of Working Modal Analysis Theory*, Electro-mechanical Engineering (in Chinese), vol. 22, no. 6, pp. 7–8 (2006).

[16] Zhou Shaoze, Zhang Jun, Zhao Wenzhong, *Research on Modal Frequency Contribution and Improvement Method of EMU Vehicle Body*, Journal of Railway Science and Engineering (in Chinese), vol. 21, no. 8 (2024).

[17] Mohsen Gerami, Navid Siahpolo, Reza Vahdani, *Effects of higher modes and MDOF on strength reduction factor of elastoplastic structures under far and near-fault ground motions*, Ain Shams Engineering Journal, vol. 8, no. 2, pp. 127–143 (2017), DOI: 10.1016/j.asej.2015.08.015.

[18] Yao Mingjing, Tang Xuan, Jia Zenghao, *Modal Analysis and Optimization Design of Frame Structure Based on CAE*, Mechanical Design and Manufacturing Engineering (in Chinese), vol. 50, no. 12, pp. 99–100 (2021).

[19] Zhou Ning, Wei Chao, Tan Mengying, *Research and Application of Testing Technology for Dynamic and Current Receiving Performance of Pantograph-catenary System*, Journal of Railway Science, vol. 42, no. 3, pp. 48–49 (2020).